

Predicting the efficacy of immune checkpoint inhibitors monotherapy in advanced non-small cell lung cancer: a machine learning method based on multidimensional data

Na LIU^{1,4,*}, Bi-Lin LIANG^{2,#}, Lu LU², Bing-Qian ZHANG^{1,4}, Jing-Jing SUN^{1,4}, Jian-Tao YANG^{1,4}, Jie XU^{2,*}, Zheng-Bo SONG^{3,4,*}, Lei SHI^{1,4,*}

¹Department of Radiology, Zhejiang Cancer Hospital, Hangzhou, Zhejiang, China; ²Shanghai Artificial Intelligence Laboratory, Shanghai, China; ³Department of Clinical Trial, Zhejiang Cancer Hospital, Hangzhou, Zhejiang, China; ⁴Institute of Basic Medicine and Cancer (IBMC), Chinese Academy of Sciences, Hangzhou, Zhejiang, China;

*Correspondence: shilei@zjcc.org.cn; songzb@zjcc.org.cn; xujie@pjlab.org.cn

#Contributed equally to this work.

Received September 8, 2022 / Accepted February 15, 2023

Immunotherapy has improved the prognosis of patients with advanced non-small cell lung cancer (NSCLC), but only a small subset of patients achieved clinical benefit. The purpose of our study was to integrate multidimensional data using a machine learning method to predict the therapeutic efficacy of immune checkpoint inhibitors (ICIs) monotherapy in patients with advanced NSCLC. We retrospectively enrolled 112 patients with stage IIIB-IV NSCLC receiving ICIs monotherapy. The random forest (RF) algorithm was used to establish efficacy prediction models based on five different input datasets, including precontrast computed tomography (CT) radiomic data, postcontrast CT radiomic data, a combination of the two CT radiomic data, clinical data, and a combination of radiomic and clinical data. The 5-fold cross-validation was used to train and test the random forest classifier. The performance of the models was assessed according to the area under the curve (AUC) in the receiver operating characteristic curve. Survival analysis was performed to determine the difference in progression-free survival (PFS) between the two groups with the prediction label generated by the combined model. The radiomic model based on the combination of precontrast and postcontrast CT radiomic features and the clinical model produced an AUC of 0.92 ± 0.04 and 0.89 ± 0.03 , respectively. By integrating radiomic and clinical features together, the combined model had the best performance with an AUC of 0.94 ± 0.02 . The survival analysis showed that the two groups had significantly different PFS times ($p<0.0001$). The baseline multidimensional data including CT radiomic and multiple clinical features were valuable in predicting the efficacy of ICIs monotherapy in patients with advanced NSCLC.

Key words: non-small cell lung cancer; immune checkpoint inhibitors; monotherapy; radiomics; machine learning

Lung cancer is the most common cancer worldwide, seriously endangering human health and life, and non-small cell lung cancer (NSCLC) accounts for 85% of lung cancers. Multiple clinical trials [1, 2] have demonstrated that immune checkpoint inhibitors (ICIs), targeting the programmed death 1 (PD-1)/programmed death ligand 1 (PD-L1) signaling pathway, have significantly improved the survival benefit of patients with advanced NSCLC, and are recommended by treatment guidelines for driver gene-negative advanced NSCLC [3]. However, only about 20% of patients with advanced NSCLC respond to ICIs monotherapy in an unselected population [4, 5]. Additionally, patients who do not respond to immunotherapy not only have expensive

drug costs but also may suffer from serious immune adverse events. Therefore, it is crucial to identify potential beneficiaries of immunotherapy early.

PD-L1 expression is the most widely used and evidence-based positive predictor of immunotherapy efficacy in NSCLC patients [6]. However, PD-L1 expression is controversial in clinical practice, and the survival benefit can also be observed in the PD-L1 negative subgroup [4]. The expression of PD-L1 in tumors is spatially and temporally heterogeneous [7]. In addition, the tumor mutation burden (TMB) [8] is currently recognized as another immunotherapy biomarker for screening potential beneficiaries with some limitations in terms of inconsistent threshold, and high detection cost.

Therefore, it is necessary to identify inexpensive, noninvasive, and easily available biomarkers to predict the efficacy of immunotherapy.

Many previous studies [9–13] have demonstrated that CT radiomics can be used as a noninvasive imaging marker to predict the outcomes of immunotherapy for NSCLC. In addition, multiple clinical factors are considered to be related to the prognosis of immunotherapy, such as histologic type [14], liver metastasis [15], and some peripheral blood inflammatory indicators [16]. Yang et al. [9] combined CT radiomics and clinicopathological characteristics to predict the clinical outcome of immunotherapy in lung cancer patients, but the study cohort, which included monotherapy and immunotherapy in combination with chemotherapy, was heterogeneous. In fact, the efficacy mechanism of chemotherapy was completely different from that of immunotherapy. Some studies [10–13] predicted the efficacy of monotherapy but did not incorporate clinical factors into the analysis. Due to tumor heterogeneity and the complex anti-tumor mechanism of immunotherapy, radiomics can only characterize the internal heterogeneity of tumor tissue, while multidimensional source data can comprehensively evaluate the biological behavior of the tumor and the physiological status of the body.

Moreover, the outcomes based on the persistence of the benefit time can more representatively reflect the real benefit of immunotherapy, eliminating patients with rare short-term reactions [17]. In clinical practice, the durable clinical benefit (DCB) is usually used to measure immunotherapy efficacy with a threshold of progression-free survival (PFS) lasting more than 6 months.

We hypothesize that the integration of multidimensional data including CT radiomics, demographic characteris-

tics, clinical characteristics, and peripheral blood indicators using a machine learning method will be able to predict immunotherapy efficacy, which is DCB in our study. In order to identify advanced NSCLC patients who will benefit from immunotherapy itself, our study only enrolled patients treated with PD-1/PD-L1 monotherapy to decrease the heterogeneity of the study cohort. A flow chart of our study is shown in Figure 1.

Patients and methods

Patients. We retrospectively included 180 patients with pathologically confirmed NSCLC between January 2016 and September 2020 in Zhejiang Cancer Hospital. The inclusion and exclusion diagrams are shown in Figure 2. The study ultimately enrolled 112 eligible patients. The Ethics Committee of Zhejiang Cancer Hospital approved this study (ethics approval number: IRB-2022-370). Written informed consent was waived by the Institutional Review Board due to the retrospective nature of the study.

Clinical features. We included a total of 20 clinical features, which were all previously reported to be associated with the prognosis of immunotherapy. The clinical features in our study included baseline demographic characteristics, clinical characteristics, and peripheral blood indicators, as follows:

The demographic and clinical characteristics included age [18], sex [19], body mass index (BMI, kg/m²) [20], smoking history [21], chronic obstructive pulmonary disease (COPD) [22], Eastern Cooperative Oncology Group (ECOG) score [23], histologic type [14], type of ICIs [24], therapy line [25], tumor stage [26], bone metastasis [27], brain metastasis [28], liver metastasis [15], and pleural effusion [29].

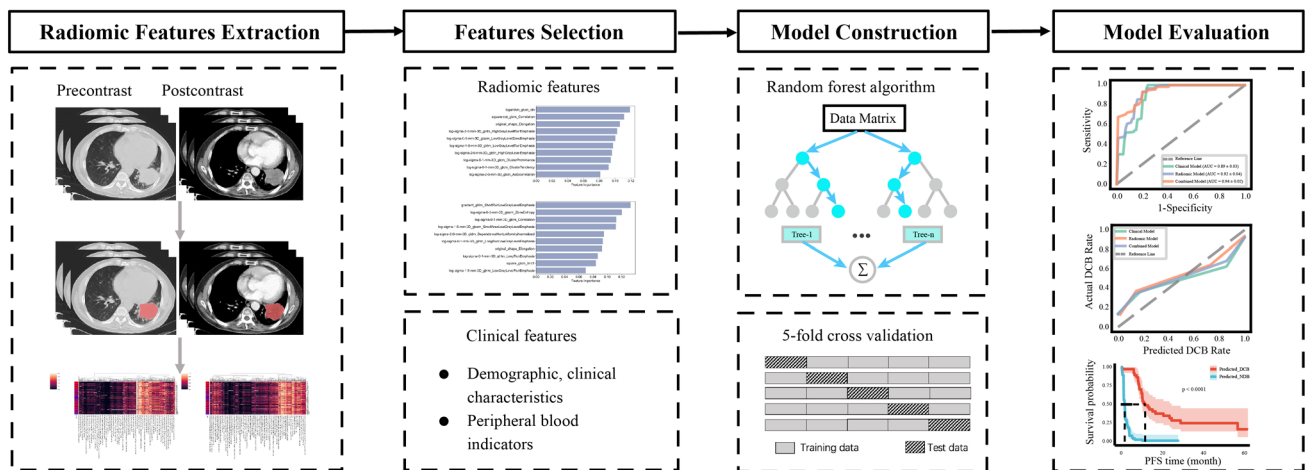


Figure 1. The flow chart of our study. The workflow includes radiomic features extraction, radiomic and clinical features selection, model construction, and model evaluation. Radiomic features extraction was carried out by manual segmentation based on precontrast CT and postcontrast CT images, respectively. The recursive feature elimination method was used to select 10 of the important radiomic features from precontrast and postcontrast radiomic data, respectively. Twenty clinical features related to efficacy were artificially selected. The random forest algorithm was used to establish prediction models, and 5-fold cross-validation was used to train and test the classifier. Finally, the performance of the models was evaluated by the receiver operating characteristic (ROC) curves and the calibration curves, and the progression-free survival (PFS) was analyzed using survival analysis.

Laboratory data were obtained within 2 weeks prior to the first ICIs treatment. The final peripheral blood indicators for data analysis included hemoglobin (g/dl) [30], serum albumin (g/dl) [31], lactate dehydrogenase (LDH) (U/l) [32], and composite inflammation indicators including the neutrophil-to-lymphocyte ratio (NLR) [16], platelet-to-lymphocyte ratio (PLR) [16], and lymphocyte-to-monocyte ratio (LMR) [33].

Efficacy evaluation criteria and follow-up. If the patients received multi-line immunotherapy, the analysis was performed using the first immunotherapy. Response assessment was based on the Response Evaluation Criteria in Solid Tumors (RECIST), version 1.1 [34], which included complete response (CR), partial response (PR), stable disease (SD), and progressive disease (PD). When the results of PD, retrospectively determined according to RECIST 1.1, were inconsistent with the results determined by clinicians based on the conditions of patients, PD cases identified by clinicians in real-time were regarded as events. The therapeutic efficacy was defined as DCB (CR, PR, or SD lasting >6 months) and no durable benefit (NDB: PD or SD lasting ≤6 months) [17]. PFS was defined as the time from the first ICIs treatment to disease progression or death from any cause, and patients without progression were censored at the time of the last clinical visit.

Image acquisition. The CT scans of all patients were acquired with a 16 or 64 row multi-slice spiral CT (Siemens SOMATOM Sensation 16; Siemens SOMATOM Definition Flash 64; GE Optima CT680). During the scan, the patients were instructed to hold their breath at the end of deep inhalation to avoid breathing motion artifacts. The tube voltage was 120 kV, and the tube current was 150–200 mAs with automatic adjustment. The pitch was 1.2–1.375. The slice thickness and slice spacing were both 5 mm. The CT images were reconstructed with a 512×512 matrix. In contrast scanning, the injection rate was 2.0–2.5 ml/s, and the injection volume was 80–100 ml. The contrast scanning was delayed by 38–40 s.

Image segmentation and feature extraction. Image segmentation and feature extraction were performed on YITU AI Enabler, using Python pyradiomics (version 3.0.1). The Feature extraction was based on Imaging Biomarker Standardization Initiative (IBSI) [35].

All imaging data were preprocessed by resampling to 1 mm × 1 mm × 1 mm voxel size to minimize the impact of different scanning protocols or equipment on quantitative radiomics analysis. The primary lung lesions were delineated as ROIs layer-by-layer for the entire tumor by a chest radiologist (Liu N). Another senior chest radiologist (Sun JJ) then confirmed and adjusted the outlined boundary. The two radiologists were both blinded to the therapeutic efficacy.

ROIs were delineated on the postcontrast CT images to avoid blood vessels and atelectasis as far as possible, and then the ROIs were copied to the precontrast CT images. Nine hundred and sixty features were first extracted from each patient based on precontrast and postcontrast CT images,

respectively. Then a feature stability check was performed with minor changes of ROIs to filter out unstable features using intraclass correlation coefficients (ICC) between the features extracted within the lesion ROIs and the extended lesion ROIs. The extended lesion ROIs were produced by extending the boundary of ROIs by 1 image pixel. The features with an ICC greater than 0.8 were preserved as stable features.

In precontrast CT images, there were 790 stable features (Supplementary Figure S1) from each patient including 14 shape features, 167 first-order statistics features, 213 gray level co-occurrence matrix (GLCM) features, 131 gray level difference matrix (GLDM) features, 155 gray level run length matrix (GLRLM) features and 110 gray level size zone matrix (GLSZM) features. In postcontrast CT images, there were 767 stable features (Supplementary Figure S2) from each patient including 14 shape features, 161 first-order statistics features, 196 GLCM features, 141 GLDM features, 151 GLRLM features, and 104 GLSZM features.

Model construction. We used recursive feature elimination (RFE) to select 10 radiomic features most related to the therapeutic efficacy from precontrast and postcontrast radiomic data, respectively. The scikit-learn package (version 1.0.2) in Python programming software (version 3.9.7) was used for model construction and evaluation. We performed random over-sampling (imblearn package; version 0.9.0) of the minority class and used these balanced datasets for developing machine learning models. All the codes are available at <https://github.com/BioAI-kits/RadClin>.

Based on the random forest (RF) algorithm, we constructed five RF models with different input datasets. The dataset and corresponding model were as follows: precontrast CT radiomic features, precontrast model; postcontrast CT radiomic features, postcontrast model; precontrast and postcontrast CT radiomic features, radiomic model; clinical features, clinical model; combined clinical and radiomic features, combined model.

We used a three-step approach to build the efficacy classification models. First, we constructed models using various combinations of tunable hyperparameters. After developing these models for each hyperparameter combination, we tested the performance of the models using the average values of AUC from 5-fold cross-validation. Finally, we selected the best hyperparameters with the highest average AUC to build models.

We evaluated the prediction performance of different models using the AUC in the ROC curves. In addition, the calibration curves were generated as a supplement to the model evaluation to visualize the goodness of fit of predictive models. The patients were divided into two groups with the prediction label (predicted DCB vs. predicted NDB), which was finally generated from the combined model. Survival analysis was performed on the PFS time of these two groups.

Statistical analysis. Comparisons of clinical features were performed using SPSS 26.0 for statistical analysis. The

continuous variables are presented as mean (standard deviation, SD) and median (interquartile range, IQR), which were compared by the independent sample t and Mann-Whitney U test. The χ^2 and Fisher's exact test were used to compare categorical variables.

Kaplan-Meier analysis was used to generate survival curves, and the log-rank test was performed to compare PFS time between the two groups on R software (survminer; version 0.4.9). All statistical analyses were two-sided and the differences were considered statistically significant at p-value <0.05.

Results

The clinical features. The baseline clinical features of the 112 patients are presented in Table 1. Thirty-nine (34.82%) patients achieved DCB, and the overall median PFS time was 2.8 months. The mean age of the patients was 59.43 years (± 7.98). There were 85 males (75.89%) and 27 females (24.11%). Fifty (44.64%) patients were diagnosed with squamous cell carcinoma (SCC), and 62 (55.36%) patients were diagnosed with non-squamous cell carcinoma (NSCC). All patients received ICIs monotherapy, including 32 (28.57%) patients treated with anti-PD-L1 drugs and 80 (71.43%) patients treated with anti-PD-1 drugs. Thirteen (11.61%) patients were treated with first-line ICIs, 85 (75.89%) patients with second-line ICIs, and 14 (12.50%) patients with third-line or above ICIs. A higher proportion of patients had stage IV tumors (90, 80.36%) than stage IIIB/IIIC tumors (22, 19.64%). There were significant differences in histologic type, tumor stage, and hemoglobin ($p=0.026$, $p=0.005$, and $p=0.044$, respectively).

The PD-L1 status was known in a small percentage of patients, including 18 (16.07%) patients with positive status and 5 (4.46%) patients with negative status. No statistical analysis of PD-L1 status was performed in this study.

Building the random forest models with different input data. The recursive elimination method was performed to select 10 of the most important features for efficacy from the precontrast and postcontrast CT radiomic dataset, respectively (Figure 3).

We further constructed five RF models with different input data, including precontrast CT radiomic features, postcontrast CT radiomic features, combined radiomic features, clinical features, combined radiomic and clinical features. The evaluation metrics of these models are shown in Table 2, and the ROC curves of each model are shown in Figure 4. The results showed that the mean AUC of the two models trained using only precontrast or postcontrast features were 0.88 ± 0.05 and 0.87 ± 0.06 , respectively. Of note, the radiomic model that was constructed with combined precontrast and postcontrast radiomic features showed better predictive performance ($AUC=0.92\pm 0.04$). The clinical model that was constructed based on various clinical features had an AUC value of 0.89 ± 0.03 . Furthermore, when clinical features

were introduced into the combined model, the predictive performance was further improved ($AUC=0.94\pm 0.02$). We also determined the goodness of fit of the radiomic model, clinical model, and combined model in the calibration curves (Figure 5A).

Applying the combined model to prognosis analysis. To quantify the contribution of individual clinical variables to efficacy prediction, we performed an interpretability analysis of the combined model. The results indicated that BMI, LMR, NLR, age, and PLR were the five most important clinical variables in efficacy prediction (Figure 5B). Furthermore, the patients were classified into two groups by the combined model: the predicted DCB group and the predicted NDB group. The survival analysis showed that PFS time between the two groups was significantly different ($p<0.0001$), with a median PFS time of 11.9 (95% CI: 10.47–24.80) months and 1.9 (95% CI: 1.43–2.07) months, respectively (Figure 6).

Discussion

The results of the present study confirmed that CT radiomics and multiple clinical data were both valuable for the efficacy prediction of immunotherapy, and the combination of the two resulted in improved prediction. Furthermore, only patients treated with PD-1/PD-L1 monotherapy were included in this study to rule out interference due to other treatments. Currently, studies predicting the efficacy of ICIs monotherapy using multidimensional data are rarely reported.

Yang et al. [36] previously used deep learning models based on multidimensional data to distinguish responders and non-responders to ICIs monotherapy at 60- and 90-days post-treatment. In terms of the time point of efficacy prediction, we assessed the therapeutic efficacy at 6 months. The efficacy was evaluated according to DCB and NDB, which is a practical and simple method for clinically classifying those who benefit from immunotherapy. The duration of the benefit time can more clearly capture the main contributor to the benefit, which is persistence. Compared with treatment response defined by the best response, DCB can not only exclude short-term responders but also accurately assess benefit in those with SD, a population with heterogeneous immunotherapy benefit profiles [17].

CT is most commonly used for tumor staging and response assessment for NSCLC in the clinic. We used two types of CT radiomic features for modeling, and our findings demonstrated that radiomic models based on precontrast or postcontrast CT radiomic features both predicted efficacy. It is known that precontrast CT radiomic features are associated with the heterogeneity of tissue density due to necrosis, hemorrhage, and myxoid changes [37], and postcontrast CT radiomic features can provide information on the spatial heterogeneity of microvascular distribution and permeability [38]. Thus, radiomic features at the macroscopic level can reflect the underlying tumor pathophysiology.

Table 1. Demographic characteristics, clinical characteristics, and peripheral blood indicators of patients.

Characteristics	Total (N = 112)	DCB (N = 39)	NDB (N = 73)	p-value
Age, mean (SD)	59.43 (7.98)	59.72 (7.96)	59.27 (8.04)	0.781
Sex, N (%)				0.115
male	85 (75.89)	33 (84.62)	52 (71.23)	
female	27 (24.11)	6 (15.38)	21 (28.77)	
BMI, mean (SD)	22.62 (2.62)	23.22 (3.36)	22.30 (2.08)	0.129
Smoking history, N (%)				0.611
yes	77 (68.75)	28 (71.79)	49 (67.12)	
no	35 (31.25)	11 (28.21)	24 (32.88)	
COPD, N (%)				0.683
yes	29 (25.89)	11 (28.21)	18 (24.66)	
no	83 (74.11)	28 (71.79)	55 (75.34)	
ECOG, N (%)				0.465
0	19 (16.96)	8 (20.51)	11 (15.07)	
1	93 (83.04)	31 (79.49)	62 (84.93)	
Histological type, N (%)				0.026*
SCC	50 (44.64)	23 (58.97)	27 (36.99)	
NSCC	62 (55.36)	16 (41.03)	46 (63.01)	
Type of ICIs, N (%)				0.950
anti-PD-L1	32 (28.57)	11 (28.21)	21 (28.77)	
anti-PD-1	80 (71.43)	28 (71.79)	52 (71.23)	
Therapy line, N (%)				0.468
1 st	13 (11.61)	6 (15.38)	7 (9.59)	
2 nd	85 (75.89)	27 (69.23)	58 (79.45)	
≥3 rd	14 (12.50)	6 (15.38)	8 (10.96)	
Tumor stage, N (%)				0.005*
IIIB	14 (12.50)	10 (25.64)	4 (5.48)	
IIIC	8 (7.14)	1 (2.56)	7 (9.59)	
IVA	43 (38.39)	17 (43.59)	26 (35.62)	
IVB	47 (41.96)	11 (28.21)	36 (49.32)	
Bone metastasis, N (%)				0.196
none	76 (67.86)	29 (74.36)	47 (64.38)	
single	11 (9.82)	5 (12.82)	6 (8.22)	
multiple	25 (22.32)	5 (12.82)	20 (27.40)	
Brain metastasis, N (%)				0.914
none	95 (84.82)	34 (87.18)	61 (83.56)	
single	6 (5.36)	2 (5.13)	4 (5.48)	
multiple	11 (9.82)	3 (7.69)	8 (10.96)	
Liver metastasis, N (%)				0.625
none	98 (87.50)	36 (92.31)	62 (84.93)	
single	3 (2.68)	1 (2.56)	2 (2.74)	
multiple	11 (9.82)	2 (5.13)	9 (12.33)	
Pleural effusion, N (%)				0.283
none	73 (65.18)	28 (71.79)	45 (61.64)	
yes	39 (34.82)	11 (28.21)	28 (38.36)	
Hemoglobin, mean (SD)	12.30 (1.49)	12.67 (1.45)	12.09 (1.48)	0.044*
Albumin, median (IQR)	4.16 (3.88; 4.35)	4.12 (3.88; 4.38)	4.16 (3.91; 4.34)	0.898
LDH, median (IQR)	224.50 (193; 298.75)	209 (184; 293)	239 (198; 335)	0.110
NLR, median (IQR)	3.24 (2.29; 4.66)	3.44 (2.25; 4.63)	3.14 (2.34; 5.00)	0.995
PLR, median (IQR)	173.00 (129.38; 229.82)	166.15 (131.50; 216.67)	185.63 (128.25; 241.00)	0.330
LMR, median (IQR)	2.41 (1.91; 3.31)	2.25 (1.83; 3.40)	2.50 (2.00; 3.25)	0.561

Note: *p<0.05; Abbreviations: SD-standard deviation; BMI-body mass index; COPD-chronic obstructive pulmonary disease; ECOG-Eastern Cooperative Oncology Group; SCC-squamous cell carcinoma; NSCC-non-squamous cell carcinoma; LDH-lactate dehydrogenase; NLR-neutrophil-to-lymphocyte ratio; PLR-platelet-to-lymphocyte ratio; LMR-lymphocyte-to-monocyte ratio; IQR-interquartile range

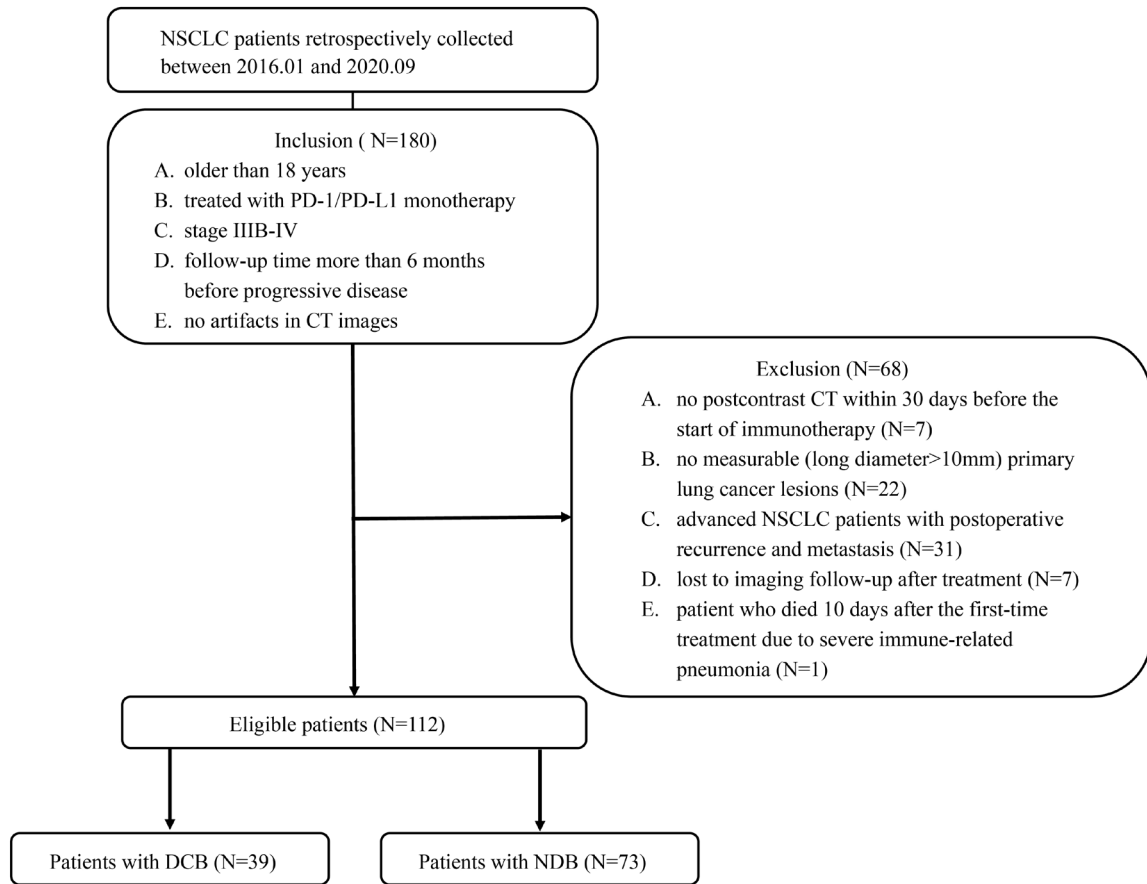


Figure 2. Inclusion and exclusion diagrams. The eligible patients were divided into two groups according to a threshold of progression-free survival (PFS) at 6 months. DCB, durable clinical benefit; NDB, no durable benefit.

Table 2. The evaluation metrics of random forest models based on different input datasets.

Model	AUC	Accuracy	Specificity	Sensitivity
Precontrast model	0.88±0.05	0.80±0.03	0.86±0.10	0.76±0.09
Postcontrast model	0.87±0.06	0.71±0.05	0.87±0.08	0.56±0.11
Radiomic model	0.92±0.04	0.80±0.03	0.84±0.10	0.76±0.09
Clinical model	0.89±0.03	0.81±0.04	0.80±0.04	0.81±0.07
Combined model	0.94±0.02	0.82±0.03	0.86±0.09	0.79±0.12

Considering that the combination of two types of CT radiomic features has the potential to comprehensively reflect tumor heterogeneity, we combined precontrast and postcontrast CT radiomic features, and the combination further improved prediction performance. The results indicated that the simultaneous application of the two types of CT radiomic features was more reliable in predicting immunotherapy efficacy. Compared with the study by Wu et al. [39], our findings further confirmed the potential advantage of the combined radiomics model to predict the efficacy of ICIs monotherapy. The immunotherapy efficacy of cohorts

with heterogeneous immunotherapy regimens including monotherapy and combined therapy may have been affected by other treatments in the study by Wu et al. In addition, Wu et al. did not combine currently known clinical biomarkers with radiomic features.

The efficacy of immunotherapy in tumors is affected by a variety of biological factors, which have a complex impact on tumor development and immune responses. A previous study [40] indicated that the predictive ability of biomarkers might be improved by the combination of different biomarkers to reduce the assumed risk associated with each one. In order to confirm the hypothesis that individual treatment response may be a comprehensive result of the interaction of various factors, we integrated multidimensional data including radiomic features, demographic characteristics, clinical characteristics, and peripheral blood indicators to predict immunotherapy efficacy. The results showed that the combination of radiomic and clinical features was better than radiomic or clinical features alone.

Machine learning methods can combine different types of features in a non-linear fashion and are able to overcome

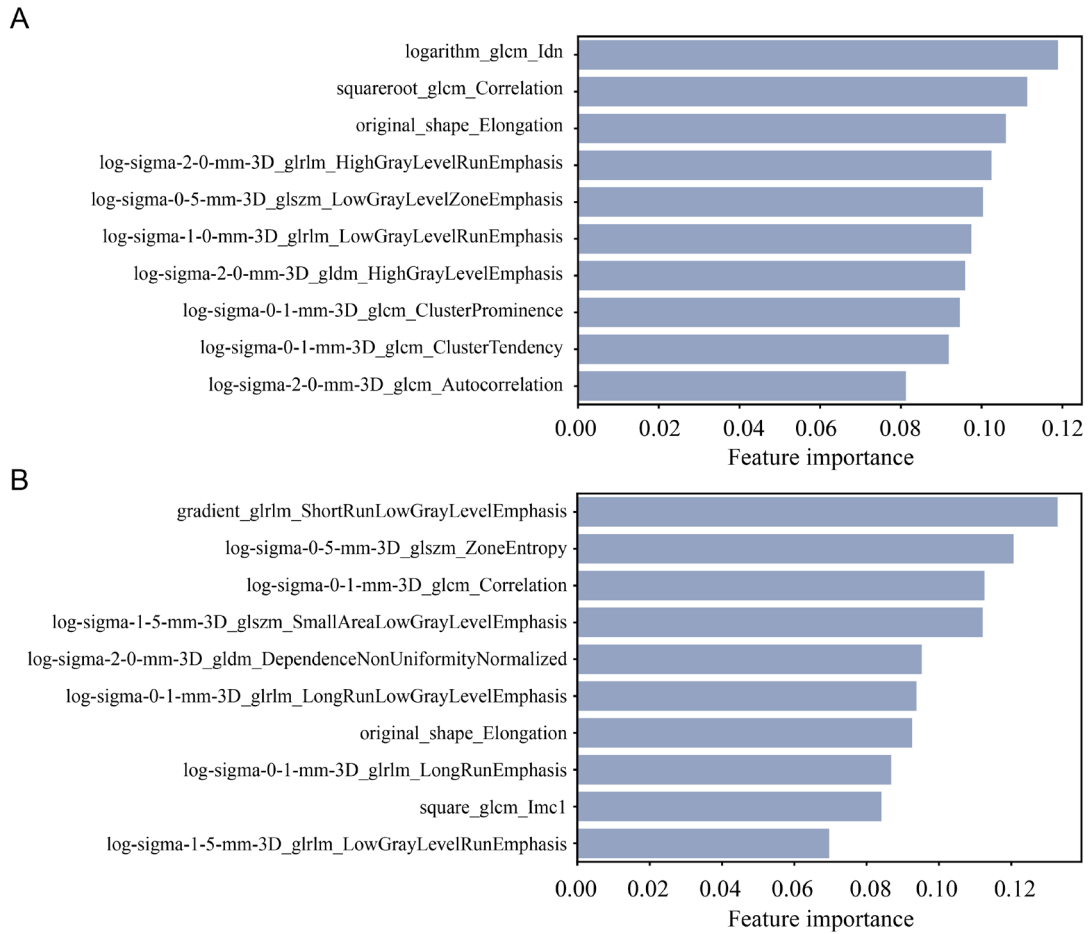


Figure 3. Radiomic features selected by recursive feature elimination. A) The top 10 most important radiomic features extracted from precontrast CT images. B) The top 10 most important radiomic features extracted from postcontrast CT images.

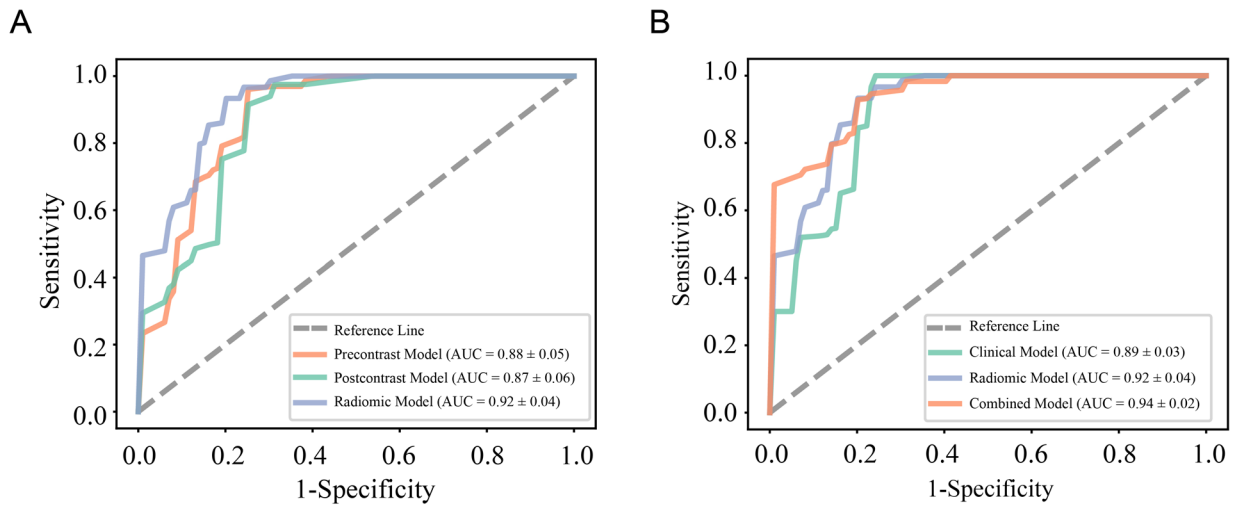


Figure 4. Receiver operating characteristic (ROC) curves for different classification models. (A) The performance of various classification models based on precontrast CT radiomic features, postcontrast CT radiomic features, and combined CT radiomic features of the two, respectively. (B) The performance of various classification models based on radiomic features, clinical features, and combined features of the two, respectively.

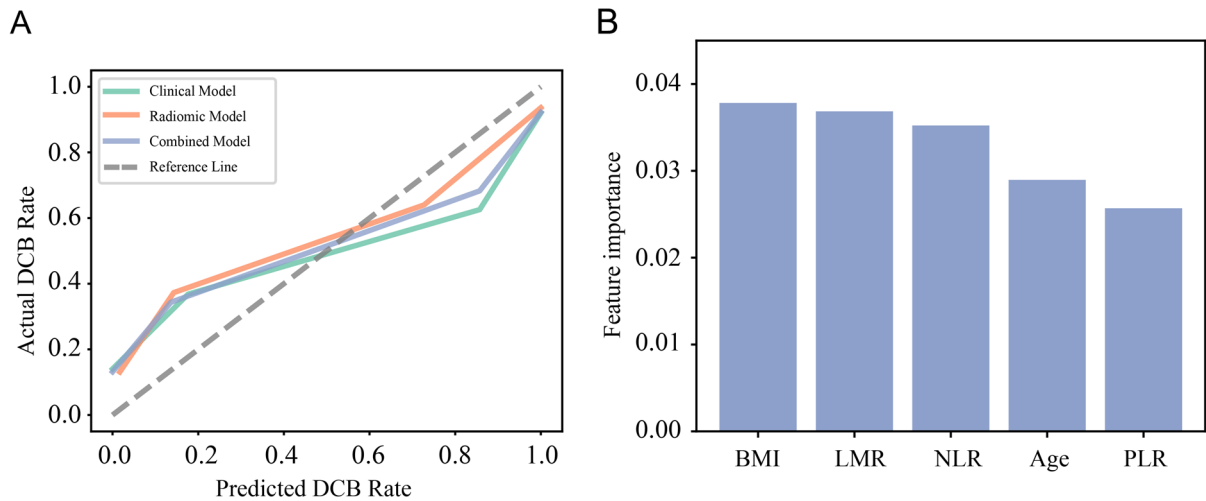


Figure 5. The goodness of fit of the classification models and interpretability analysis of the combined model. A) Calibration curves for the clinical model, radiomic model, and combined model. B) Feature importance weight plot: the top five clinical variables most important for efficacy prediction in the combined model.

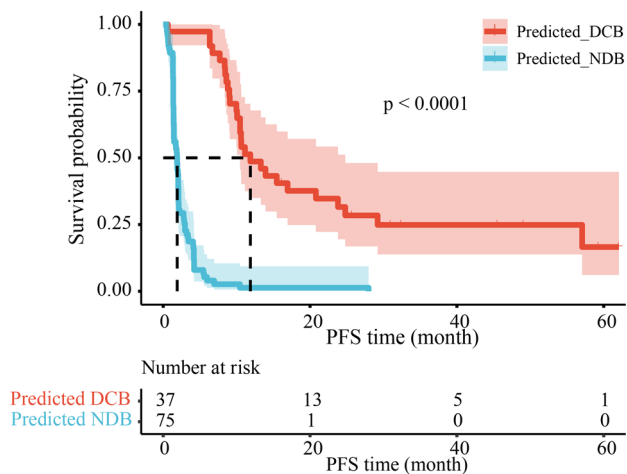


Figure 6. Kaplan-Meier survival curve. Survival analysis of PFS time in the two groups (predicted DCB vs. predicted NDB by the combined model).

the limitations of predictors that rely on a single feature [41]. The study by Chowell et al. [41] revealed that the non-linear combination of multiple features had different degrees of contribution to the overall prediction of response. In our study, the top five most important clinical features associated with therapeutic efficacy using the RF classifier were BMI, LMR, NLR, age, and PLR, which are known to provide information on nutrition, immune, and inflammatory status. A previous study [42] demonstrated that nutrition status can affect tumor development and response to treatment, and is closely related to the prognosis of cancer patients. Elderly patients tend to develop immunosenescence, which is charac-

terized by a decline in immune capacity with increasing age [43]. Inflammation can promote or induce tumor initiation, progression, and metastasis by regulating the tumor micro-environment [42]. An increasing number of studies [16, 33] have demonstrated that LMR, NLR, and PLR are biomarkers, which reflect the level of systemic inflammation, and can represent the balance between promoting tumor response and antitumor immune function. Additionally, these potential prognostic factors are noninvasive, inexpensive, and routinely obtained in clinical practice.

Our study had several limitations: Firstly, this was a retrospective study with a small sample size in a single center and there was no external validation dataset. As it was difficult to identify a PD-1/PD-L1 monotherapy cohort with complete clinical and imaging data at baseline, we failed to find homogenization data in multiple centers. However, we believe that our findings will motivate more researchers to further examine this issue. Secondly, overall survival (OS) data were not used in the analysis as the majority of patients received subsequent multi-line therapy after immunotherapy. Thirdly, recent research [44] showed that several gene alterations (such as EGFR-mutant, ROS1 rearrangement, HER2 mutation) may affect the efficacy of immunotherapy in NSCLC. Unfortunately, we lack sequencing data to analyze their role in predicting the efficacy of immunotherapy.

In conclusion, this preliminary exploratory study demonstrated that CT features combined with multiple biological factors were valuable for predicting the efficacy of PD-1/PD-L1 monotherapy in patients with advanced NSCLC. The results are expected to provide a basis for the establishment of a multidimensional model based on clinical and laboratory indicators in addition to imaging features for subsequent researchers.

Acknowledgments: We thank International Science Editing (<http://www.internationalscienceediting.com>) for editing this manuscript. This work was supported by grants from the Natural Science Foundation of Zhejiang Province (Grant Number: Y22H227294), the Medical Science and Technology Project of Zhejiang Province (Grant Number: 2022KY097, 2022RC114).

Supplementary information is available in the online version of the paper.

References

- [1] AGUIAR PN JR, DE MELLO RA, BARRETO CMN, PERRY LA, PENNY-DIMRI J et al. Immune checkpoint inhibitors for advanced non-small cell lung cancer: emerging sequencing for new treatment targets. *ESMO Open* 2017; 2: e000200. <https://doi.org/10.1136/esmoopen-2017-000200>
- [2] TANG S, QIN C, HU H, LIU T, HE Y et al. Immune Checkpoint Inhibitors in Non-Small Cell Lung Cancer: Progress, Challenges, and Prospects. *Cells* 2022; 11: 320. <https://doi.org/10.3390/cells11030320>
- [3] HANNA NH, ROBINSON AG, TEMIN S, BAKER S JR, BRAHMER JR et al. Therapy for Stage IV Non-Small-Cell Lung Cancer With Driver Alterations: ASCO and OH (CCO) Joint Guideline Update. *J Clin Oncol* 2021; 39: 1040–1091. <https://doi.org/10.1200/JCO.20.03570>
- [4] BRAHMER J, RECKAMP KL, BAAS P, CRINO L, EBERHARDT WE et al. Nivolumab versus Docetaxel in Advanced Squamous-Cell Non-Small-Cell Lung Cancer. *N Engl J Med* 2015; 373: 123–135. <https://doi.org/10.1056/NEJMoa1504627>
- [5] BORGHAEI H, PAZ-ARES L, HORN L, SPIGEL DR, STEINS M et al. Nivolumab versus Docetaxel in Advanced Nonsquamous Non-Small-Cell Lung Cancer. *N Engl J Med* 2015; 373: 1627–1639. <https://doi.org/10.1056/NEJMoa1507643>
- [6] ETTINGER DS, WOOD DE, AISNER DL, AKERLEY W, BAUMAN JR et al. NCCN Guidelines Insights: Non-Small Cell Lung Cancer, Version 2.2021. *J Natl Compr Canc Netw* 2021; 19: 254–266. <https://doi.org/10.6004/jnccn.2021.0013>
- [7] HONG L, NEGRAO MV, DIBAJ SS, CHEN R, REUBEN A et al. Programmed Death-Ligand 1 Heterogeneity and Its Impact on Benefit From Immune Checkpoint Inhibitors in NSCLC. *J Thorac Oncol* 2020; 15: 1449–1459. <https://doi.org/10.1016/j.jtho.2020.04.026>
- [8] HELLMANN MD, CIULEANU TE, PLUZANSKI A, LEE JS, OTTERSON GA et al. Nivolumab plus Ipilimumab in Lung Cancer with a High Tumor Mutational Burden. *N Engl J Med* 2018; 378: 2093–2104. <https://doi.org/10.1056/NEJMoa1801946>
- [9] YANG B, ZHOU L, ZHONG J, LV T, LI A et al. Combination of computed tomography imaging-based radiomics and clinicopathological characteristics for predicting the clinical benefits of immune checkpoint inhibitors in lung cancer. *Respir Res* 2021; 22: 189. <https://doi.org/10.1186/s12931-021-01780-2>
- [10] KHORRAMI M, PRASANNA P, GUPTA A, PATIL P, VELU PD et al. Changes in CT Radiomic Features Associated with Lymphocyte Distribution Predict Overall Survival and Response to Immunotherapy in Non-Small Cell Lung Cancer. *Cancer Immunol Res* 2020; 8: 108–119. <https://doi.org/10.1158/2326-6066.CIR-19-0476>
- [11] VAIDYA P, BERA K, PATIL PD, GUPTA A, JAIN P et al. Novel, non-invasive imaging approach to identify patients with advanced non-small cell lung cancer at risk of hyper-progressive disease with immune checkpoint blockade. *J Immunother Cancer* 2020; 8: e001343. <https://doi.org/10.1136/jitc-2020-001343>
- [12] LIU C, GONG J, YU H, LIU Q, WANG S et al. A CT-Based Radiomics Approach to Predict Nivolumab Response in Advanced Non-Small-Cell Lung Cancer. *Front Oncol* 2021; 11: 544339. <https://doi.org/10.3389/fonc.2021.544339>
- [13] GRANATA V, FUSCO R, COSTA M, PICONE C, COZZI D et al. Preliminary Report on Computed Tomography Radiomics Features as Biomarkers to Immunotherapy Selection in Lung Adenocarcinoma Patients. *Cancers (Basel)* 2021; 13: 3992. <https://doi.org/10.3390/cancers13163992>
- [14] ZHENG Q, HUANG Y, ZENG X, CHEN X, SHAO S et al. Clinicopathological and molecular characteristics associated with PD-L1 expression in non-small cell lung cancer: a large-scale, multi-center, real-world study in China. *J Cancer Res Clin Oncol* 2021; 147: 1547–1556. <https://doi.org/10.1007/s00432-020-03444-y>
- [15] QIAO M, ZHOU F, HOU L, LI X, ZHAO C et al. Efficacy of immune-checkpoint inhibitors in advanced non-small cell lung cancer patients with different metastases. *Ann Transl Med* 2021; 9: 34. <https://doi.org/10.21037/atm-20-1471>
- [16] DIEM S, SCHMID S, KRAPF M, FLATZ L, BORN D et al. Neutrophil-to-Lymphocyte ratio (NLR) and Platelet-to-Lymphocyte ratio (PLR) as prognostic markers in patients with non-small cell lung cancer (NSCLC) treated with nivolumab. *Lung Cancer* 2017; 111: 176–181. <https://doi.org/10.1016/j.lungcan.2017.07.024>
- [17] RIZVI H, SANCHEZ-VEGA F, LA K, CHATILA W, JONSSON P et al. Molecular Determinants of Response to Anti-Programmed Cell Death (PD)-1 and Anti-Programmed Death-Ligand 1 (PD-L1) Blockade in Patients With Non-Small-Cell Lung Cancer Profiled With Targeted Next-Generation Sequencing. *J Clin Oncol* 2018; 36: 633–641. <https://doi.org/10.1200/JCO.2017.75.3384>
- [18] NISHIJIMA TE, MUSS HB, SHACHAR SS, MOSCHOS SJ. Comparison of efficacy of immune checkpoint inhibitors (ICIs) between younger and older patients: A systematic review and meta-analysis. *Cancer Treat Rev* 2016; 45: 30–37. <https://doi.org/10.1016/j.ctrv.2016.02.006>
- [19] CONFORTI F, PALA L, BAGNARDI V, DE PAS T, MARTINETTI M et al. Cancer immunotherapy efficacy and patients' sex: a systematic review and meta-analysis. *Lancet Oncol* 2018; 19: 737–746. [https://doi.org/10.1016/S1470-2045\(18\)30261-4](https://doi.org/10.1016/S1470-2045(18)30261-4)

- [20] KICHENADASSE G, MINERS JO, MANGONI AA, ROWLAND A, HOPKINS AM et al. Association Between Body Mass Index and Overall Survival With Immune Checkpoint Inhibitor Therapy for Advanced Non-Small Cell Lung Cancer. *JAMA Oncol* 2020; 6: 512–518. <https://doi.org/10.1001/jamaoncol.2019.5241>
- [21] NORUM J, NIEDER C. Tobacco smoking and cessation and PD-L1 inhibitors in non-small cell lung cancer (NSCLC): a review of the literature. *ESMO Open* 2018; 3: e000406. <https://doi.org/10.1136/esmoopen-2018-000406>
- [22] ZHOU J, CHAO Y, YAO D, DING N, LI J et al. Impact of chronic obstructive pulmonary disease on immune checkpoint inhibitor efficacy in advanced lung cancer and the potential prognostic factors. *Transl Lung Cancer Res* 2021; 10: 2148–2162. <https://doi.org/10.21037/tlcr-21-214>
- [23] SPIGEL DR, MCCLEOD M, JOTTE RM, EINHORN L, HORN L et al. Safety, Efficacy, and Patient-Reported Health-Related Quality of Life and Symptom Burden with Nivolumab in Patients with Advanced Non-Small Cell Lung Cancer, Including Patients Aged 70 Years or Older or with Poor Performance Status (CheckMate 153). *J Thorac Oncol* 2019; 14: 1628–1639. <https://doi.org/10.1016/j.jtho.2019.05.010>
- [24] DUAN J, CUI L, ZHAO X, BAI H, CAI S et al. Use of Immunotherapy With Programmed Cell Death 1 vs Programmed Cell Death Ligand 1 Inhibitors in Patients With Cancer: A Systematic Review and Meta-analysis. *JAMA Oncol* 2020; 6: 375–384. <https://doi.org/10.1001/jamaoncol.2019.5367>
- [25] WU S, WANG L, LI W, CHEN B, LIU Y et al. Comparison between the first-line and second-line immunotherapy drugs in the progression-free survival and overall survival in advanced non-small cell lung cancer: a systematic review and meta-analysis of randomized controlled trials. *Ann Palliat Med* 2021; 10: 1717–1726. <https://doi.org/10.21037/apm-20-449>
- [26] WU J, XU C, GUAN X, NI D, YANG X et al. Comprehensive analysis of tumor microenvironment and identification of an immune signature to predict the prognosis and immunotherapeutic response in lung squamous cell carcinoma. *Ann Transl Med* 2021; 9: 569. <https://doi.org/10.21037/atm-21-463>
- [27] ZHU YJ, CHANG XS, ZHOU R, CHEN YD, MA HC et al. Bone metastasis attenuates efficacy of immune checkpoint inhibitors and displays “cold” immune characteristics in Non-small cell lung cancer. *Lung Cancer* 2022; 166: 189–196. <https://doi.org/10.1016/j.lungcan.2022.03.006>
- [28] ZHOU S, XIE J, HUANG Z, DENG L, WU L et al. Anti-PD-(L)1 immunotherapy for brain metastases in non-small cell lung cancer: Mechanisms, advances, and challenges. *Cancer Lett* 2021; 502: 166–179. <https://doi.org/10.1016/j.canlet.2020.12.043>
- [29] EPAILLARD N, BENITEZ JC, GORRIA T, FABRE E, RIU-DAVETS M et al. Pleural effusion is a negative prognostic factor for immunotherapy in patients with non-small cell lung cancer (NSCLC): The pluie study. *Lung Cancer* 2021; 155: 114–119. <https://doi.org/10.1016/j.lungcan.2021.03.015>
- [30] ZHANG Z, ZHANG F, YUAN F, LI Y, MA J et al. Pre-treatment hemoglobin level as a predictor to evaluate the efficacy of immune checkpoint inhibitors in patients with advanced non-small cell lung cancer. *Ther Adv Med Oncol* 2020; 12: 1758835920970049. <https://doi.org/10.1177/1758835920970049>
- [31] YOO SK, CHOWELL D, VALERO C, MORRIS LGT, CHAN TA. Pre-treatment serum albumin and mutational burden as biomarkers of response to immune checkpoint blockade. *NPJ Precis Oncol* 2022; 6: 23. <https://doi.org/10.1038/s41698-022-00267-7>
- [32] MEZQUITA L, AUCLIN E, FERRARA R, CHARRIER M, REMON J et al. Association of the Lung Immune Prognostic Index With Immune Checkpoint Inhibitor Outcomes in Patients With Advanced Non-Small Cell Lung Cancer. *JAMA Oncol* 2018; 4: 351–357. <https://doi.org/10.1001/jamaoncol.2017.4771>
- [33] SEKINE K, KANDA S, GOTO Y, HORINOUCHE H, FUJIWARA Y et al. Change in the lymphocyte-to-monocyte ratio is an early surrogate marker of the efficacy of nivolumab monotherapy in advanced non-small-cell lung cancer. *Lung Cancer* 2018; 124: 179–188. <https://doi.org/10.1016/j.lungcan.2018.08.012>
- [34] EISENHAUER EA, THERASSE P, BOGAERTS J, SCHWARTZ LH, SARGENT D et al. New response evaluation criteria in solid tumours: revised RECIST guideline (version 1.1). *Eur J Cancer* 2009; 45: 228–247. <https://doi.org/10.1016/j.ejca.2008.10.026>
- [35] ZWANENBURG A, VALLIERES M, ABDALAH MA, AERTS H, ANDREARCZYK V et al. The Image Biomarker Standardization Initiative: Standardized Quantitative Radiomics for High-Throughput Image-based Phenotyping. *Radiology* 2020; 295: 328–338. <https://doi.org/10.1148/radiol.2020191145>
- [36] YANG Y, YANG J, SHEN L, CHEN J, XIA L et al. A multi-omics-based serial deep learning approach to predict clinical outcomes of single-agent anti-PD-1/PD-L1 immunotherapy in advanced stage non-small-cell lung cancer. *Am J Transl Res* 2021; 13: 743–756.
- [37] GANESHAN B, ABALEKE S, YOUNG RC, CHATWIN CR, MILES KA. Texture analysis of non-small cell lung cancer on unenhanced computed tomography: initial evidence for a relationship with tumour glucose metabolism and stage. *Cancer Imaging* 2010; 10: 137–143. <https://doi.org/10.1102/1470-7330.2010.0021>
- [38] WIN T, MILES KA, JANES SM, GANESHAN B, SHASTRY M et al. Tumor heterogeneity and permeability as measured on the CT component of PET/CT predict survival in patients with non-small cell lung cancer. *Clin Cancer Res* 2013; 19: 3591–3599. <https://doi.org/10.1158/1078-0432.CCR-12-1307>
- [39] WU M, ZHANG Y, ZHANG J, ZHANG Y, WANG Y et al. A Combined-Radiomics Approach of CT Images to Predict Response to Anti-PD-1 Immunotherapy in NSCLC: A Retrospective Multicenter Study. *Front Oncol* 2021; 11: 688679. <https://doi.org/10.3389/fonc.2021.688679>

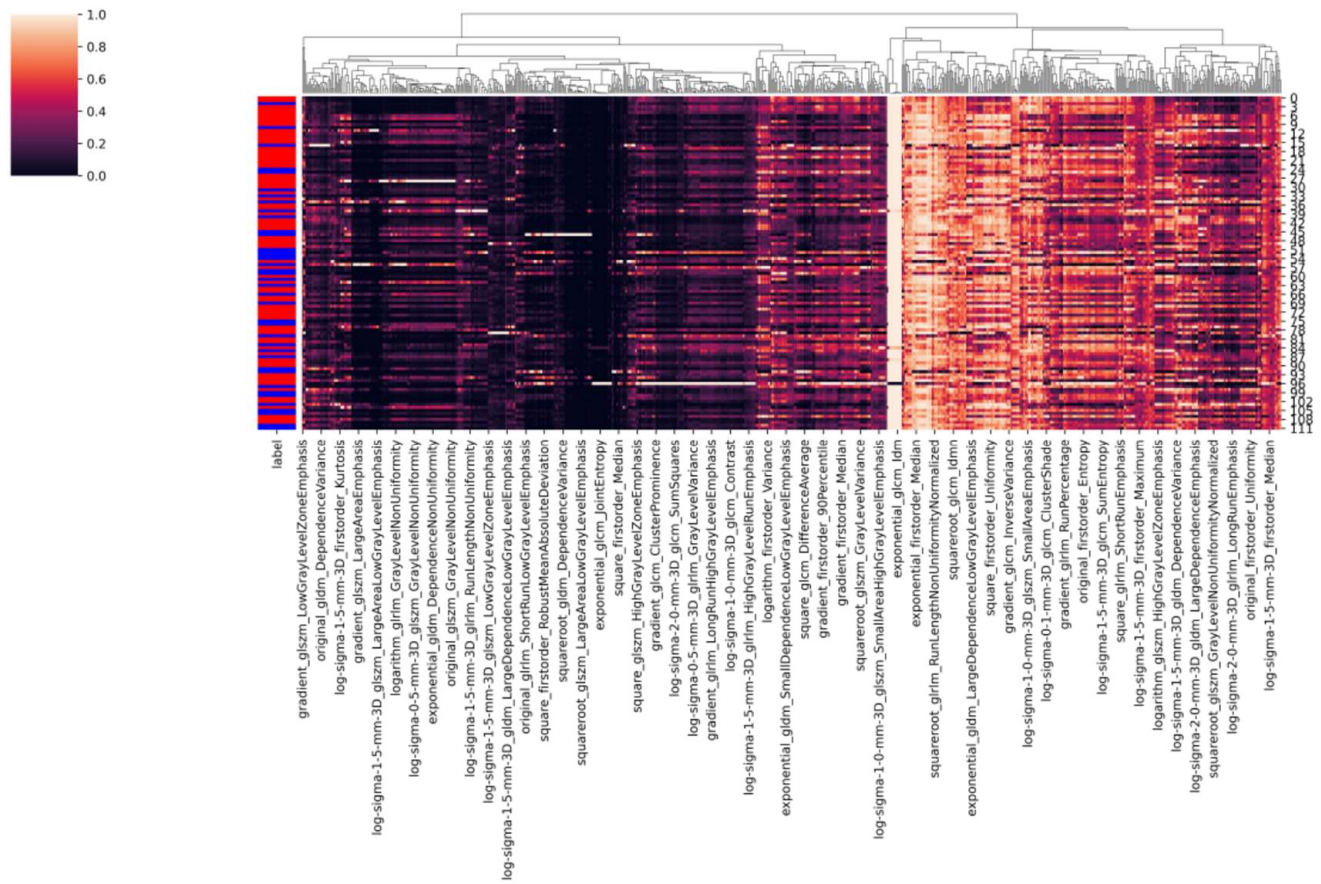
- [40] CAMIDGE DR, DOEBELE RC, KERR KM. Comparing and contrasting predictive biomarkers for immunotherapy and targeted therapy of NSCLC. *Nat Rev Clin Oncol* 2019; 16: 341–355. <https://doi.org/10.1038/s41571-019-0173-9>
- [41] CHOWELL D, YOO SK, VALERO C, PASTORE A, KRISHNA C et al. Improved prediction of immune checkpoint blockade efficacy across multiple cancer types. *Nat Biotechnol* 2022; 40: 499–506. <https://doi.org/10.1038/s41587-021-01070-8>
- [42] ZITVOGEL L, PIETROCOLA F, KROEMER G. Nutrition, inflammation and cancer. *Nat Immunol* 2017; 18: 843–850. <https://doi.org/10.1038/ni.3754>
- [43] PAWELEC G, DERHOVANESSIAN E, LARBI A. Immunosenesence and cancer. *Crit Rev Oncol Hematol* 2010; 75: 165–172. <https://doi.org/10.1016/j.critrevonc.2010.06.012>
- [44] GUO X, DU H, LI J, YANG M, XIONG A et al. Efficacy of ICIs on patients with oncogene-driven non-small cell lung cancer: a retrospective study. *Cancer Drug Resist* 2022; 5: 15–24. <https://doi.org/10.20517/cdr.2021.85>

https://doi.org/10.4149/neo_2023_220908N912

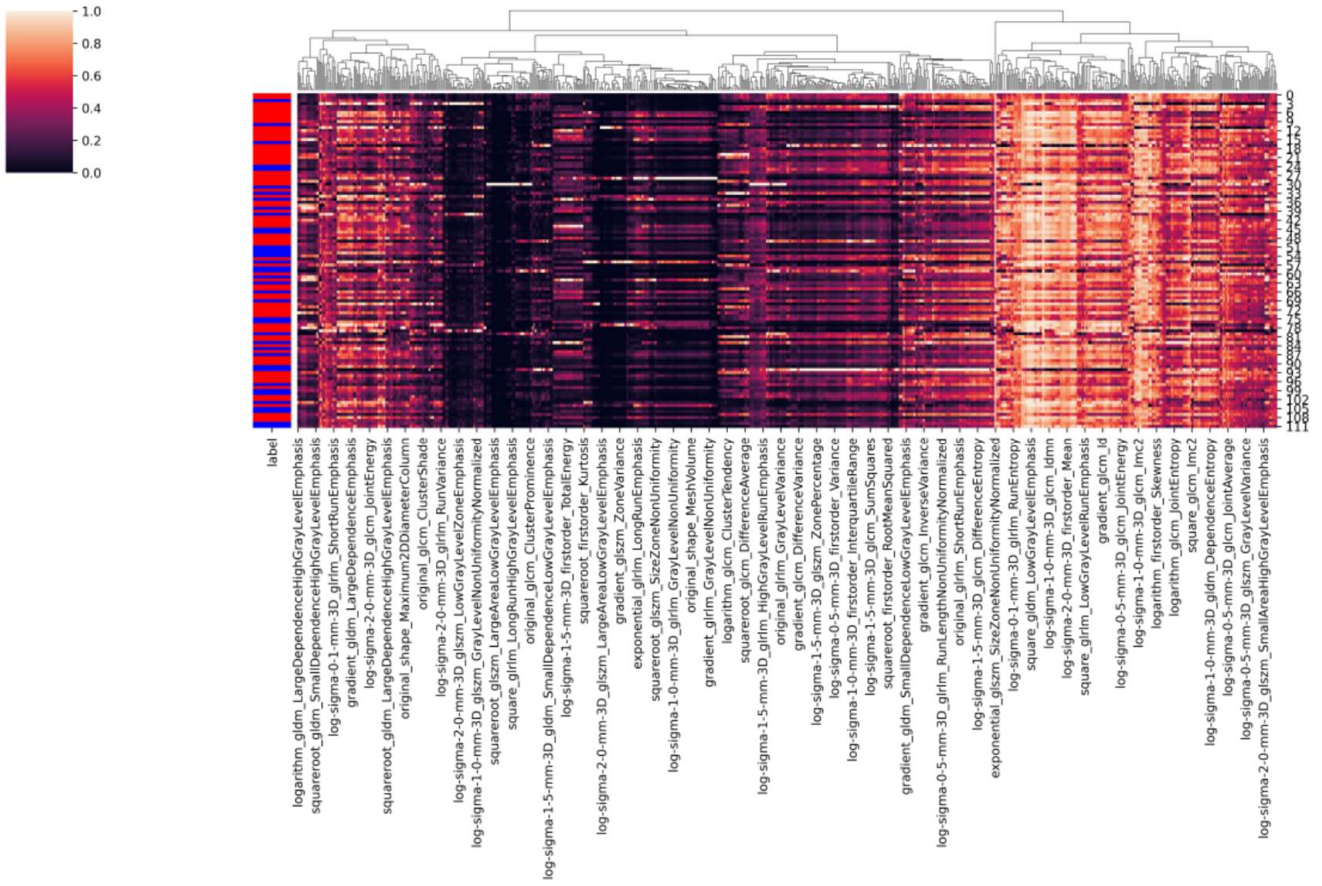
Predicting the efficacy of immune checkpoint inhibitors monotherapy in advanced non-small cell lung cancer: a machine learning method based on multidimensional data

Na LIU^{1,4,*}, Bi-Lin LIANG^{2,*}, Lu LU², Bing-Qian ZHANG^{1,4}, Jing-Jing SUN^{1,4}, Jian-Tao YANG^{1,4}, Jie XU^{2,*}, Zheng-Bo SONG^{3,4,*}, Lei SHI^{1,4,*}

Supplementary Information



Supplementary Figure S1. The heatmap of 790 radiomic features in precontrast CT.



Supplementary Figure S2. The heatmap of 767 radiomic features in postcontrast CT.